ChemElectroChem

Research Article
doi.org/10.1002/celc.202200109

Chemistry Europe
European Chemical Societies Publishing

www.chemelectrochem.org

Special Collection

# Statistical Analysis of the Measurement Noise in Dynamic Impedance Spectra

Richard Chukwu, John Mugisa, Doriano Brogioli, and Fabio La Mantia*[a]

Different strategies can be used to acquire dynamic impedance spectra during a cyclic voltammetry experiment. The spectra are then analyzed by fitting them with a model using a weighted non-linear least-squares minimization algorithm. The choice of the weighting factors is not trivial and influences the value of the extracted parameters. At variance with the classic electrochemical impedance spectroscopy, dynamic impedance measurements are performed under non-stationary conditions, making them typically more prone to errors arising from the voltage and current analog-to-digital conversion. Under the assumption that the noise in the voltage and current signals have a constant variance along the measurement and that it is uncorrelated between distinct samples, we calculate an expression for the expected variance of the error of the resulting immittances, which considers the specific procedure used to extract the spectra under the time-varying nature of the measurements. The calculated variance of the error is then used as a rigorous way to evaluate the weighting factors of the least-squares minimization, assuming that the fitted model is ideally exact and that there are no systematic errors. By exploring two classical electrochemical systems and fitting the measured spectra with a transfer function measurement model, namely with the Padé approximants, we show that the variance evaluated with our method captures the frequency dependence of the resulting residuals and can be used for reliably performing the complex non-linear least-squares fitting procedure.

## Introduction

Dynamic impedance spectroscopy (dEIS) is a technique that makes it possible to capture the time-dependent frequency response of an electrochemical system under non-stationary conditions.[1–4] dEIS features the use of multi-sine excitation to perturb a non-linear time-varying system and subsequent extraction of the spectra via Fourier transform techniques. Often, dEIS performs the time-resolved impedance measurements[5] during the classic cyclic voltammetry (CV): it allows the complete measurement of a sequence of spectra during the period of the cyclic voltammetry scan; thus, each spectrum can be attributed to a phase (cathodic or anodic scan) or a polarization potential of the electrode. Various strategies for the evaluation of dynamic impedance spectra have been developed.[6] Dynamic multi-frequency analysis (DMFA),[1,6,7] is the underlying strategy employed in this study to extract impedance spectra obtained under dynamic conditions. A more traditional technique is the Fast Fourier transform electrochemical impedance spectroscopy.[3,8,9] DMFA has been successfully employed in the extraction of spectra obtained from EIS studies on redox couples, hydrogen evolution, and intercalation of cations in thin films of $LiMn_2O_4$[10] and nickel hexacyanoferrate.[11]

Higher errors usually characterize spectra obtained from dEIS compared to the spectra obtained in the static mode. In the latter method, one frequency is injected at a time so that the measuring device automatically optimizes the current range of the acquisition for each measured frequency.[11] This optimization is relevant because the measurement noise changes with the current range approximately linearly. By contrast, dEIS uses a single current acquisition range matching the sum of all the frequencies, which is much larger than the current range needed for measuring a single frequency. The preceding situation leads to relatively more significant measurement noise and, in turn, larger error on the measured impedance spectra.

After the acquisition of an impedance spectrum, a process or measurement model is typically used to fit the acquired data by means of a regression. The process models include physical models (models derived from physical principles) and equivalent circuits,[12,13] where the parameters obtained provide some information about the physico-chemical properties of the electrochemical system under study. The measurement models include the Voigt measurement model developed by Agarwal et al.[14–16] which uses a Voigt series (a series connection containing a number of resistors (R) and capacitors (C) elements in parallel), and the Transfer function measurement model introduced by L. Pauwels et al.[17] which involves the use of Padé approximants.[18,17] Measurement models aim to identify spectra characteristics to facilitate selecting an appropriate process model. Padé approximants used in the study are rational functions in $\sqrt{j\omega}$, where $j$ represents the imaginary number and $\omega$ is the angular frequency. These rational

[a] R. Chukwu, J. Mugisa, Dr. D. Brogioli, Prof. F. L. Mantia
Universität Bremen
Energiespeicher- und Energiewandlersysteme
Bibliothekstr. 1, 28359 Bremen, Germany
E-mail: lamantia@uni-bremen.de

Supporting information for this article is available on the WWW under https://doi.org/10.1002/celc.202200109

An invited contribution to the Wolfgang Schuhmann Festschrift

functions serve as generalized measurement models and allow a general description of the immittance spectra in the whole range of frequencies investigated.[19] Hence, they can also be used when you do not have a direct physical model in mind. Furthermore, when the electrochemical system under study is known and can be described by an equivalent circuit, the conversion between the elements of the equivalent circuit and coefficients of the Padé approximants is possible. Van Gheem et al.[20] describes the methodology to obtain an equivalent circuit based on a rational function while further details are provided by Zoltowski[19,21] and Sadkowski.[22] An added advantage of measurement models is that even when the electrochemical system is a black box, some information such as the ohmic resistance and capacitance and polarization impedance of the electrochemical system can be obtained.[21,23]

The procedure for fitting the experimental data with a model requires knowledge of the distribution of errors inherent in the data. By means of this knowledge, the likelihood of a model can be quantitatively evaluated; that is, the most likely physical parameter values will be considered the most reliable estimate. If the errors are independent and normally distributed, the maximization of the likelihood function is practically performed via a least-squares fit. The weights used in the complex non-linear least squares fit are chosen to be proportional to the inverse of the variance of the errors in the spectra.[24–26] Qualitatively, this definition of weights places lower reliance on the data with the largest uncertainty.[27] It is thus clear that, in order to obtain a reliable, meaningful and mathematically sound evaluation of the fit parameters, the statistical distribution of the errors of the fitted experimental data must be measured or calculated.

For practical reasons, a simple error evaluation approach was to assume the standard deviation of the impedance is proportional to the modulus of the impedance.[28] A study by Jennings and Wang[29] showed that weighting impedance data obtained for Dye-sensitized solar cells using the modulus gave similar results to weighting using the experimentally obtained variance. However, they also report that the parameters obtained from the modulus weighting scheme are not the optimal in terms of the maximum likelihood principle. Other studies also confirm that weighting by the variance yields much more reliable information. Two key bodies of work are those by Jansen et al.[30] on thermally stimulated deep-level impedance spectroscopy and Orazem et al.[31] on the application of measurement models to electrohydrodynamic impedance spectroscopy. In both studies, weighting by the variance of the errors increased the quality of the information obtained from the physical parameters.

The straightforward approach to identifying the error variance in measurements would be to take replicate measurements; however, this method is more prone to errors arising from unwanted long-term drifts of the experimental conditions. An analysis procedure that allowed the assessment of the variance of the errors from semi-replicate or sequential impedance measurements was developed by Orazem et al.[31–33] This method is based on the assumption that the variance of the residual fitting errors can provide a reasonable estimate for the variance of the errors in the impedance data. In their approach, the Voigt series with the same number of elements is fitted to each impedance measurement in order to filter out the drift and lack of replicacy. An empirical expression that relates the standard deviation of the impedance to the real part, imaginary part and magnitude of the impedance is then used to model the residuals' standard deviation. The expression also contains four unknown constants, which must be evaluated by an iterative loop; this allows an "a posteriori" evaluation of the errors.[23,29]

To address the problem of taking repeated measurements as described in the preceding paragraph, we propose a more direct approach towards estimating the stochastic error based on an assumption of the distribution of the noise in the acquired signals (current and voltage). We assume that the variance of the noise in the voltage and current is constant and independent of time. We derive an expression for the error on the admittance from the principles of error propagation. We show that the variance of the error of the admittance, measured through DMFA, depends on the squared absolute value of the admittance, the amplitude of the multi-sine voltage signal, the shape of the filter function used, and the variance of the noise of the acquired voltage and current signals. Although a similar expression could be derived for the impedance, we chose the admittance in this study because, rigorously, the transfer function is the ratio between the response and stimulus. Since we operated in potentiostatic mode, the stimulus is a potential oscillation, and the response is a current oscillation: the transfer function is the admittance.

After providing the formula for evaluating "a priori" the variance of the error, for the case of DMFA, we use it as proper weighting for the regression of Padé approximants to experimental spectra. Two experimental systems are considered: The ferri/ferrocyanide $[Fe(CN)_6]^{3-/4-}$ redox system (referred to as the redox system) and the intercalation of potassium ions into nickel hexacyanoferrate (NiHCF) nanoparticles (from now on referred to as the intercalation system). These two electrochemical systems have been widely studied in the literature[34–36] and are well suited for the analysis described in this study.

Our approach offers another benefit besides the fact that we are able to extract the variance of the errors in the admittance. In dEIS, there is a trade-off between the speed of the measurements and the accuracy of spectrum points,[4] hence the parameters of the multi-sine have to be chosen carefully. Armed with the knowledge of the expected standard deviation, our expression allows us to reverse engineer the design of the multi-sine signal such that the ratio of the variance of the error on the admittance to the absolute value of the admittance does not vary significantly within the spectrum.

## Dynamic multi-frequency analysis: analysis procedure

The three-electrode electrochemical cell containing the system under study is connected to a potentiostat. Next, we perturb the system with a signal comprising a quasi-triangular cyclic voltammetry (quasi-CV) waveform superimposed with a multi-

sine.[1] A quasi-CV waveform was chosen over the classic triangular waveform to avoid the Gibb's phenomenon.[37] Discrete samples of the working electrode voltage versus the reference $v_n$ and the current response $i_n$ signals are then acquired with an analog to digital converter connected to a potentiostat. Further details on the experimental setup are described under the experimental section, while details of the quasi-CV waveform and multi-sine design can be found elsewhere.[1]

After we obtain $v_n$ and $i_n$, we proceed to calculate their discrete-time Fourier transform of the acquired voltage $V_k$ and current $I_k$ measured at frequency $F_k$, where $k$ represents the index of the frequency.

$$V_k = \frac{1}{\sqrt{N}} \sum_{n=0}^{N-1} v_n \cdot \exp\left(-j2\pi \frac{k \cdot n}{N}\right) \tag{1}$$

$$I_k = \frac{1}{\sqrt{N}} \sum_{n=0}^{N-1} i_n \cdot \exp\left(-j2\pi \frac{k \cdot n}{N}\right) \tag{2}$$

It is worth noting that the symbols $v_n$ and $i_n$ represent the signals in the time domain while $V_k$ and $I_k$ represent the signals in the frequency domain. The next stage is splitting the frequency domain into several signals: one around the zero frequency, representing the quasi-CV component, and others representing the waves of the multi-sine perturbation. This operation is performed by using a band-pass filter $g(\mathrm{k}-\mathrm{k}_0)$ mathematically represented as:

$$\begin{aligned} g(k-k_0) = {} & [1+\exp(-n_b)]^2 / \\ & \left[1+\exp\left(-n_b \cdot \frac{(F_b \cdot k - F_b \cdot k_0) + w_b}{w_b}\right)\right] / \\ & \left[1+\exp\left(n_b \cdot \frac{(F_b \cdot k - F_b \cdot k_0) - w_b}{w_b}\right)\right] \end{aligned} \tag{3}$$

Where $F_b$ represents the base frequency ($\frac{1}{N \cdot \Delta t}$), $N$ is the length of the signal, $\Delta t$ is the time interval, $n_b$ is a factor that describes the shape of the filter function and is taken to be equal to 8 in this study and $w_b$ is the bandwidth. The choice of the values between 8 and 16 is a good compromise between the broadening in the shape of the filter and the minimization of oscillations. With this value of $n_b$, the band-pass filter has a flat-top with a shape that lies between gaussian and perfectly rectangular (see Figure 1a and 1b of the supporting information). For every acquired frequency denoted by index $k$, and for the quasi-CV component around the zero frequency, the signal is calculated by multiplying the Fourier transform of the signal, $V_k$ and $I_k$, times $g(k-k_0)$. After this filtering operation, a single frequency $F_k$ is preserved in the signal, along with the information on the amplitude and phase modulations up to the frequency $w_b$.[6]

The next step in the DMFA process is the calculation of the dynamic admittance $Y_{l,k_0}$. In this step, every frequency section elaborated in the previous step is transformed back into the time domain via the inverse discrete-time Fourier transform. Dynamic admittance spectra can be defined through the ratio of the filtered inverse discrete-time Fourier transform of current and the voltage represented by the symbols $\tilde{i}_{l,k_0}$ and $\tilde{v}_{l,k_0}$. The value of the filtered inverse discrete-time Fourier transform of the voltage around the frequency index $k_0$ is given by:

$$\tilde{v}_{l,k_0} = \frac{1}{\sqrt{N}} \sum_{k=N/2}^{N/2-1} V_k \cdot g(k-k_0) \cdot \exp\left(j2\pi \frac{k \cdot l}{N}\right) \tag{4}$$

Substituting the right-hand side of Equation (1) as $V_k$ into Equation (4) and simplifying further yields:

$$\tilde{v}_{l,k_0} = \frac{1}{\sqrt{N}} \sum_{n=0}^{N-1} \left[ v_n \frac{1}{\sqrt{N}} \sum_{k=N/2}^{N/2-1} \left\{ g(k-k_0) \cdot \exp\left(-j2\pi \frac{k \cdot (n-l)}{N}\right) \right\} \right] \tag{5}$$

Equation (5) can be rewritten in a shorter form as:

$$\tilde{v}_{l,k_0} = \frac{1}{\sqrt{N}} \sum_{n=0}^{N-1} v_n \cdot f(n-l,k_0) \cdot \exp\left(-j2\pi \frac{k_0 \Delta n}{N}\right) \tag{6}$$

Where:

$$\begin{aligned} f(\Delta n, k_0) = {} & \frac{1}{\sqrt{N}} \sum_{k=-N/2}^{N/2-1} \left[ g(k-k_0) \cdot \exp\left(-j2\pi \frac{k \Delta n}{N}\right) \right] \\ & \cdot \exp\left(j2\pi \frac{k_0 \Delta n}{N}\right) \end{aligned} \tag{7}$$

and $\Delta n = n - l$. Here we see that $f(\Delta i, k_0)$ is actually the Fourier transform of $g(k)$ multiplied by a phase factor depending on $k_0$. Since $g(k-k_0)$ vanishes for values of $k$ far from $k_0$, it is possible to decrease the range of the sum given in Equation (7):

$$\begin{aligned} f(\Delta n, k_0) = {} & \frac{1}{\sqrt{N}} \sum_{k=k_0-M/2}^{k_0+M/2-1} \left[ g(k-k_0) \cdot \exp\left(-j2\pi \frac{k \Delta n}{N}\right) \right] \\ & \cdot \exp\left(j2\pi \frac{k_0 \Delta n}{N}\right) \end{aligned} \tag{8}$$

Where $M$ is a number larger than the bandwidth of the filter $g(k)$ but smaller than $N$. By substituting the variable $k$ as $k_0 + k'$, we arrive at:

$$f(\Delta n) = \frac{1}{\sqrt{N}} \sum_{k'=-M/2}^{M/2-1} g(k') \cdot \exp\left(-j2\pi \frac{k' \Delta n}{N}\right) \tag{9}$$

Here we see that $f$ does not actually depend on $k_0$ thus we write $f$ only as a function of $\Delta n$. Following from Equation (9) the values of the filtered inverse discrete-time Fourier transform of the voltage and the current are represented by:

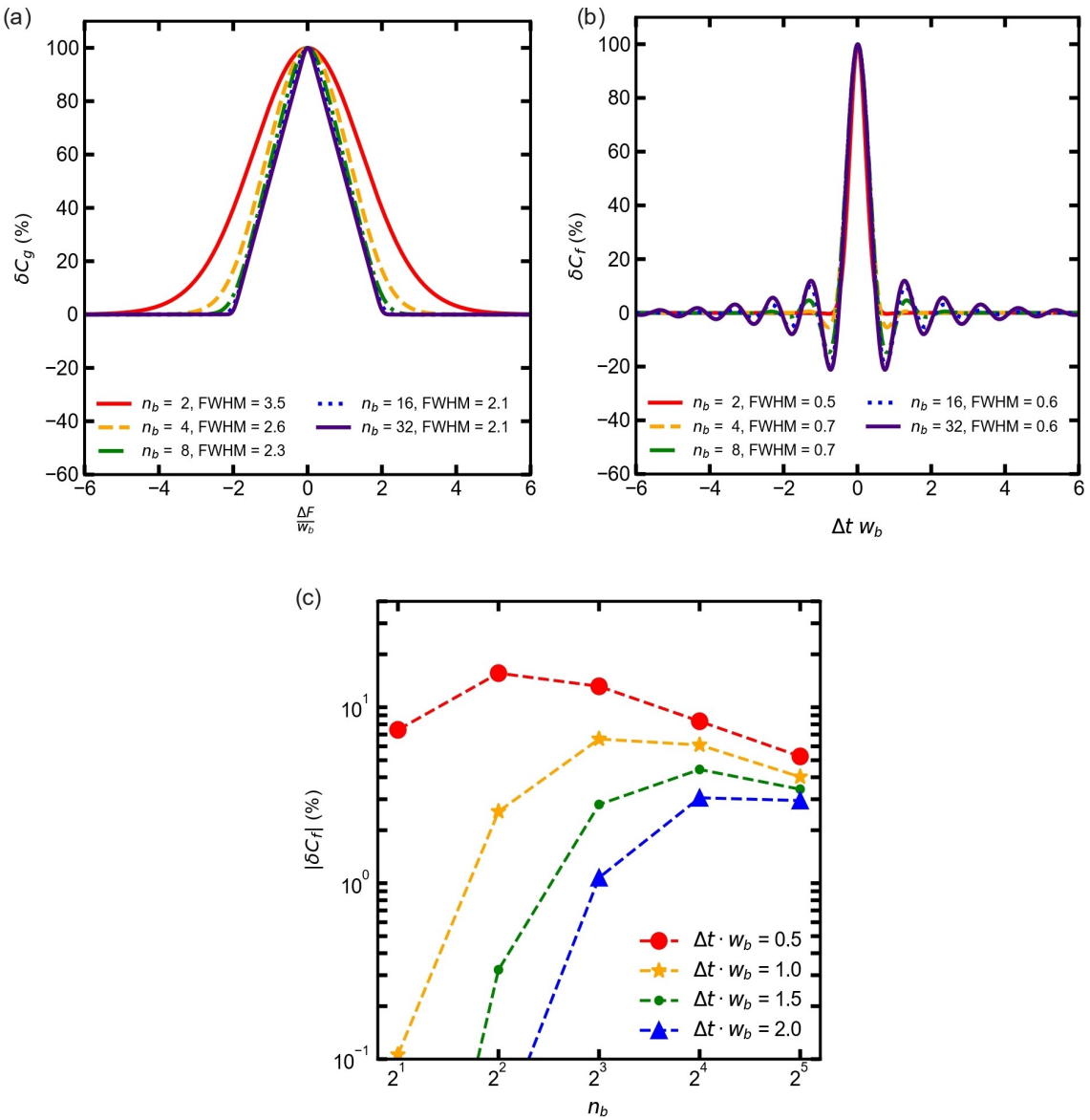


**Figure 1.** Plots of (a) correlation between the errors on admittances obtained at two frequencies $\delta \boldsymbol{C}_g$ vs $\frac{\Delta F}{w_b}$ with varing filter parameter $\boldsymbol{n}_b$ (b) correlation between the errors on admittances obtained at two different times $\delta \boldsymbol{C}_f$ vs $\Delta t \cdot \boldsymbol{w}_b$ with varing filter parameter $\boldsymbol{n}_b$ (c) absolute percentage correlation between the errors on admittances obtained at two different times $\delta \boldsymbol{C}_f$ vs $\boldsymbol{n}_b$ with varing $\Delta t \cdot \boldsymbol{w}_b$.

$$\tilde{v}_{l,k_0} \frac{1}{\sqrt{N}} \sum_{n=0}^{N-1} v_n \cdot f(n-l) \cdot \exp\left(-j2\pi \frac{k_0 \Delta n}{N}\right) \tag{10}$$

$$\tilde{i}_{l,k_0} = \frac{1}{\sqrt{N}} \sum_{n=0}^{N-1} i_n \cdot f(n-l) \cdot \exp\left(-j2\pi \frac{k_0 \Delta n}{N}\right) \tag{11}$$

The admittance $Y_{l,k_0}$ is finally defined as the ratio between $\tilde{i}_{l,k_0}$ and $\tilde{v}_{l,k_0}$:

$$Y_{l,k_0} = \frac{\tilde{i}_{l,k_0}}{\tilde{v}_{l,k_0}} \tag{12}$$

Substituting the right-hand side of Equations (10) and (11), respectively, for $\tilde{v}_{l,k_0}$ and $\tilde{i}_{l,k_0}$ and substituting $\theta_{k_0,\Delta n}$ for $\exp\left(-j2\pi \frac{k_0 \Delta n}{N}\right)$ gives:

$$Y_{l,k_0} = \frac{\sum_{n=0}^{N-1} i_n \cdot f(n-l) \cdot \theta_{k_0,\Delta n}}{\sum_{n=0}^{N-1} v_n \cdot f(n-l) \cdot \theta_{k_0,\Delta n}} \tag{13}$$

In order to evaluate the expected variance of the error on the admittance, $\sigma^2_{Y\,l,k_0}$, we employ the propagation of error formulas.[38] In particular, we assume that the noise of the voltage and current is time-independent and has an approximately Gaussian distribution with variance $\sigma_v^2$ and $\sigma_i^2$, respec-

tively. Thus, the expected variance of the error on the real $\sigma^2_{\mathrm{Re}(Y)}$ and imaginary $\sigma^2_{\mathrm{Im}(Y)}$ parts of the admittance are given by:

$$\sigma^2_{\mathrm{Re}(Y)} = \sum_{m=0}^{N-1}\left|\frac{\partial \mathrm{Re}(Y)}{\partial i_m}\right|^2 \sigma_i^2 + \left|\frac{\partial \mathrm{Re}(Y)}{\partial v_m}\right|^2 \sigma_v^2 \tag{14}$$

$$\sigma^2_{\mathrm{Im}(Y)} = \sum_{m=0}^{N-1}\left|\frac{\partial \mathrm{Im}(Y)}{\partial i_m}\right|^2 \sigma_i^2 + \left|\frac{\partial \mathrm{Im}(Y)}{\partial v_m}\right|^2 \sigma_v^2 \tag{15}$$

In the present study, we also make use of equality of the variance of the errors on the real $\sigma^2_{\mathrm{Re}(Y)}$ and imaginary $\sigma^2_{\mathrm{Im}(Y)}$ parts of the admittance since the admittance Y is an analytic function of the Fourier transform of the signals $I_k$ and $V_k$ and drawing on the fact that the noise on the signals $i_n$ and $v_n$ is preserved during the Fourier transform (see supporting information – section 1.1). For the sake of simplicity, we shall drop the subscripts Re and Im and denote the variance of the error on either the real or imaginary part of the dynamic admittance as $\sigma^2_{Y_{l,k_0}}$. Thus, we can combine Equations (14) and (15) into a single equation and consider half the value as being the variance of the error in either the real or the imaginary components of the admittance.,

$$\sigma^2_{Y_{l,k_0}} = \frac{1}{2}\sum_{m=0}^{N-1}\left|\frac{\partial \mathrm{Re}\left(Y_{l,k_0}\right)}{\partial i_m}\right|^2 \sigma_i^2 + \left|\frac{\partial \mathrm{Re}\left(Y_{l,k_0}\right)}{\partial v_m}\right|^2 \sigma_v^2 \tag{16}$$

Substituting the corresponding partial derivatives yields:

$$\sigma^2_{Y_{l,k_0}} = \frac{1}{2}\left(\sigma_i^2 \sum_{m=0}^{N-1}\left|\frac{f(m-l)\cdot\theta_{k_0,m-l}}{\sum_{n=0}^{N-1} v_n \cdot f(n-l)\cdot\theta_{k_0,n-l}}\right|^2 + \sigma_v^2 \sum_{m=0}^{N-1}\left|\frac{f(m-l)\cdot\theta_{k_0,m-l}\sum_{n=0}^{N-1} i_n \cdot f(n-l)\cdot\theta_{k_0,n-l}}{\left(\sum_{n=0}^{N-1} v_n \cdot f(n-l)\cdot\theta_{k_0,n-l}\right)^2}\right|^2\right) \tag{17}$$

Factoring and simplifying Equation (17) further gives:

$$\sigma^2_{Y_{l,k_0}} = \frac{1}{2}\left(\frac{\sum_{m=0}^{N-1}\left|f(m-l)\right|^2}{\left|\sum_{n=0}^{N-1} v_n \cdot f(n-l)\cdot\theta_{k_0,n-l}\right|^2}\left[\sigma_i^2 + \sigma_v^2\left|Y_{l,k_0}\right|\right]\right) \tag{18}$$

Finally, rewriting Equation (18) in terms of Equation (5) under that the assumption that the norm $\sum_{m=0}^{N-1}|f|^2$ is preserved by the Fourier transform $\sum_{k=-N/2}^{N/2}|g|^2$ and using basic algebraic manipulations, we arrive at a final expression for $\sigma^2_{Y_{l,k_0}}$ as:

$$\sigma^2_{Y_{l,k_0}} = \frac{\sigma_i^2 + \left|Y_{l,k_0}\right|^2 \sigma_v^2}{2N'\left|\tilde{v}_{l,k_0}\right|^2} \tag{19}$$

where the value of $N'$ is given by:

$$N' = \frac{N}{\sum_{k=-N/2}^{N/2}\left|g\left(k-k_0\right)\right|^2} \tag{20}$$

$N$ is the length of the signal and $k$ indexes the discrete frequencies. The value of $N'$ depends on the shape and bandwidth of the filter function, and it is a number larger than one. Equation (19) shows that the variance is composed of two parts, a constant one and another, proportional to the squared absolute value of the admittance. Further details on the derivation are given in section 1 of the supporting information.

In order to reliably obtain the maximally likely parameters by means of a least-squares fit, the weights must be assigned based on the variances; however, we also need a second condition which is the independence of the errors of the admittances $Y_{l,k_0}$. While the noise on the original signals are uncorrelated, the process of obtaining the spectra via DMFA introduces some correlation between the errors on the extracted admittances. Nevertheless, we can choose the parameters used in the extraction of the admittance such that this correlation in the time and frequency domains are brought to a minimum. The degree of correlation (expressed in percentage) as a function of various parameters is illustrated in Figure 1. Taking two distinct values of $k_0$, say $k_0^1$ and $k_0^2$, the errors on $Y_{l,k_0^1}$ and $Y_{l,k_0^2}$ are uncorrelated provided that the difference between corresponding frequencies $F_{k_0^1} - F_{k_0^2}$ much larger than $w_b$ (see supporting information – section 1.2). The choice of the multi-sine signal of the DMFA and the filter bandwidth $w_b$ is made in order to meet this requirement.

Similarly, the errors on the admittances $Y_{l^1,k_0}$ and $Y_{l^2,k_0}$ evaluated at different time indexes $l^1$ and $l^2$ are independent and uncorrelated if the distance is much less than the width of the filter function $f(m-l)$ in time, i.e. if $l^2 - l^1$ ($\Delta t$) is much more than the inverse of the filter bandwidth $w_b$ (see supporting information – section 1.3); thus, care must be taken when the time dependence is analyzed. In practice, the absolute value of the correlation of the errors on the admittance obtained at two distinct times, $\delta C_f$, is less than 20% when successive impedances are distant more than $0.5/w_b$ apart, as shown in Figure 1c.

## Results and Discussion

### Determination of $\sigma_i$ and $\sigma_v$

To obtain $\sigma_V$ and $\sigma_I$, we conducted a series of voltage and current measurements across different resistors with resistance ranging from 10 $\Omega$ to 2 $k\Omega$. We applied zero volts across the

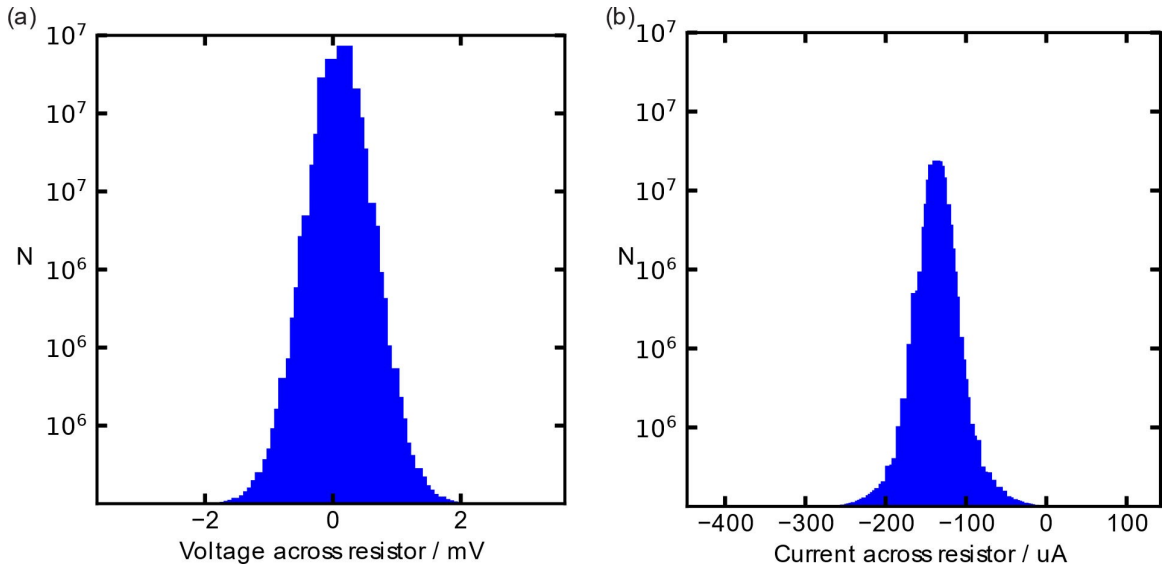


**Figure 2.** Histogram showing the distribution of 100 million points of (a) voltage and (b) current across a 20 $\Omega$ resistor.

resistors and measured the voltage and the current response. The resulting histogram of the voltage and the current measurement presented in Figure 2 shows that both quantities are approximately Gaussian. Nevertheless, there was no implicit assumption of the probability distributions in our derivation since we relied only on the first and second moments. Furthermore, the distributions of the inverse discrete-time Fourier transform of the current and the voltage, represented by the symbols $\tilde{i}_{l,k_0}$ and $\tilde{v}_{l,k_0}$, have normal distributions as a consequence of the central limit theorem.[39] It was also found that $\sigma_i$ scaled linearly with the current range as shown in Figure S11 of the supporting information. The values of $\sigma_i$ and $\sigma_v$ used in this study are listed in Table 1.

We tested two experimental systems: the ferric-/ferrocyanide redox system and the intercalation of potassium ions into nickel hexacyanoferrate particles as described in the experimental section. We performed the DMFA procedure and extracted 50 spectra each from the cathodic scans of both systems for the present analysis. Fitting of the series of spectra obtained from the dynamic impedance measurements was achieved via regression of Padé approximants of sequentially increasing orders beginning from order three. The weights used in the regression were chosen to be inversely proportional to the variance obtained in Equation (19). Plots of the experimental data and the final fit with a Padé orders three for the redox system and five for the intercalation system are shown for select voltage points in Figure 3(a) and Figure 3(b).

**Table 1.** Summary of DMFA parameters used in the acquisition of dynamic admittance.

| DEIS Parameters | Redox | Intercalation |
|---|---|---|
| $E_h$ [V] | 0.25 | 0.1 |
| Scan rate [mV/s] | 60 | 5 |
| $\Delta U_{dc}$ [mVpp] | 250 | 400 |
| $F_b$ [Hz] | 1 | 0.5 |
| $\Delta U_{ac}$ [mVpp] | 50 | 50 |
| No of points (x$10^6$) | 200 | 800 |
| Sample rate [$\mu s$] | 0.2 | 0.4 |
| Current range [mA] | 1 | 100 |
| $w_b$ [Hz] | 0.5 | 0.25 |
| $\sigma_V$ [V] | 5.6e–04 | 5.2e–04 |
| $\sigma_I$ [A] | 3.37e–07 | 3.1e–05 |

In order to ensure that a more parsimonious model was selected during regression of the transfer function measurement model, the Akaike information criterion (AIC)[40] and the Bayesian information criterion (BIC)[41] were used. These criteria mentioned can provide an effective method to compare models and weighting techniques in impedance data analysis.[26] The AIC considers the goodness of fit, which increases with an increasing number of parameters, $p$, and the model complexity:[26]

$$\mathrm{AIC} = -2\ln\hat{L} + 2p \tag{21}$$

The first term $-2\ln\hat{L}$ contains the log-likelihood estimator, which is maximised under the central assumption of normally distributed residuals when the sum of squares in the least-squares estimator is minimised. The AIC gives us a strategy to avoid under- and over-fitting.[42,43] Underfitting occurs when the fitted expression fails to identify effects that were supported by the data, i.e., high bias – low variance. In contrast, overfitting occurs when the fitted expression contains spurious variables and is characterised by low bias-high variance. When the variance in the experimental data is known, the AIC is given by:

$$\mathrm{AIC} = n_f \ln(2\pi) + \sum_{i=1}^{n_f} \ln\sigma_i^2 + \sum_{i=1}^{n_f} \chi^2 + 2p \tag{22}$$

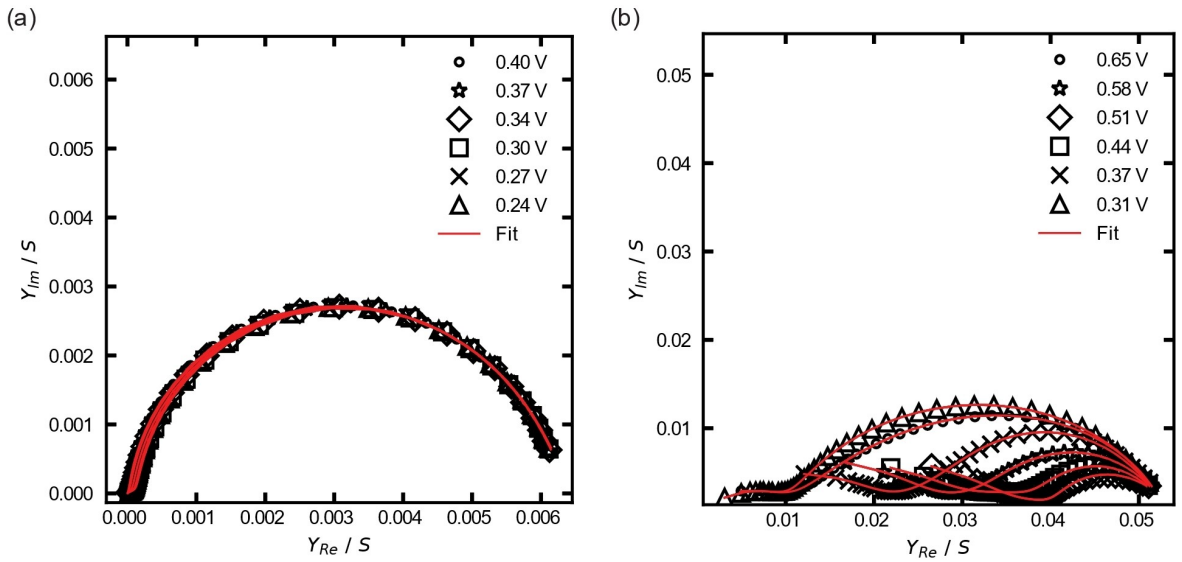


**Figure 3.** Admittance plots obtained for (a) reduction of ferricyanide at a platinum disk electrode (redox system) (b) the intercalation of potassium ions into NiHCF particles (intercalation system). The red line represents the fit using Padé order three for the redox system and Padé order five for the intercalation system.

where the value of $n_f$ represents the length of frequency points, $\chi^2$ represents the weighted residual sum of squares and p represents the model parameters. Thus, the AIC provides the benefit of penalising additional parameters without requiring the use of confidence intervals and additional statistical tests.[26] The BIC is given by:

$$\mathrm{BIC} = n_f \ln(2\pi) + \sum_{i=1}^{n_f} \ln \sigma_i^2 + \sum_{i=1}^{n_f} \chi^2 + p \ln n_f \qquad (23)$$

The AIC and the BIC were used to select the appropriate Padé approximant order (simply referred to as Padé order) used in the regression. The final Padé order chosen was the one for which the average AIC was minimum based on the information provided in Figure 4. The order with the minimum AIC corresponds to the model with parameters identical to the classical maximum likelihood estimate. This minimum value was obtained for Padé order three for the redox system and Padé order five for the intercalation system. The value of the AICc, which is the AIC with a bias correction for small degrees of freedom and the weighted chi-square were also calculated. Details of the values of the AIC, BIC, AICc and weighted chi-

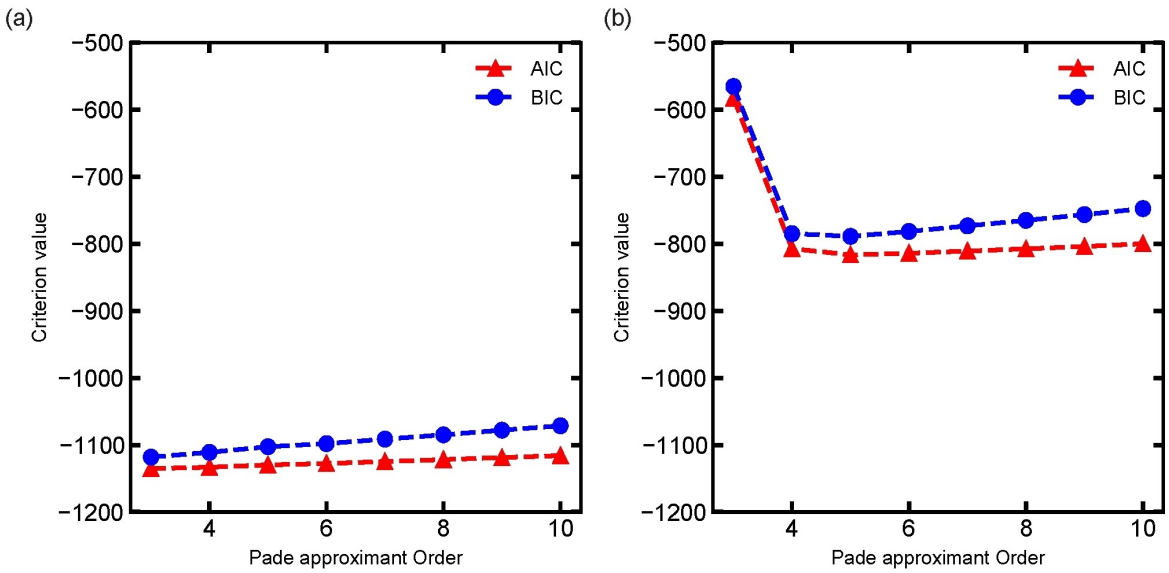


**Figure 4.** Bias variance plot showing the values of the Akaike information criterion (AIC) and Bayesian information criterion (BIC) as a function of the Padé approximant order for (a) the redox system and (b) the intercalation system.

square employed in this study are listed in Table S1 and S2 of the supporting information. The Akaike weights, $W_i$ also presented in Table S3 and Table S4 of the supporting information were used to evaluate the level of confidence in the choice of the Padé order used in the subsequent analysis.

Once a suitable approximant order was chosen, we evaluated the residuals and the corresponding standard deviations on the real and imaginary parts of the admittance from the square root of the variance of the residuals using Equation (24) under suitable assumptions.[15,44]

$$\sigma_r^2 = \frac{1}{N_s - 1}\sum_{i}^{N_s}\left(\varepsilon_{res,\mathrm{Re}(Y_{i,k})} - \overline{\varepsilon}_{res,\mathrm{Re}(Y_k)}\right)^2 \tag{24}$$

Where $N_s$ is the number of measurements, and $\varepsilon_{res,\mathrm{Re}(Y_{i,k})}$ represents the residuals (difference between the experimental and calculated admittance) for spectra $Y_i$ obtained at frequency $k$. A similar expression was used to calculate the standard deviation of the imaginary part of the admittance $\sigma_j$.

The array of normalized residual elements (i.e. residuals normalized by $\sigma_Y$) obtained for the regression to the set of 50 spectra for redox and intercalation systems were plotted as a function of frequency and voltage. The plots for redox and intercalation systems are depicted respectively in Figures S3 and S7 of the supporting information. No significant systematic deviations were recorded. We went further to calculate, for every frequency measured, the weighted standard deviations (using residuals normalized by the standard deviation calculated from Equation (19)) of the real and imaginary parts of the admittance. A similar calculation was done for every voltage measured. The resulting plots are shown in Figure 5. Again, the results show a clear trend with frequency as the weighted standard deviations presented in Figure 5(a) and Figure 5(b) had values up to four times the expected value at lower frequencies for both systems. In general, there appeared to be a spike in values at lower frequencies of the spectrum. When plotted as a function of the voltage, the weighted standard deviation of the real and imaginary parts of the admittance ranged between one and three-and-half times of the expected value. The expected value is one. Thus, the observed larger values represent the extent of the discrepancy between the measured values and that estimated by Equation (19).

Normalizing the standard deviations to the magnitude of the admittance Figure 6(a) and Figure 6(b) yields the scaled standard deviations which represent the relative error in the measurement. It can be seen that the error ranges from 0.02% to 0.5% of the modulus for the redox system and between 0.02% to 0.1% of the modulus for the intercalation system.

In Figure 7(a) and Figure 7(b), the residual standard deviations for the redox and intercalation systems are plotted as a function of frequency. Solid green lines denote data for the mean of $\sigma_Y$ across the voltages for each frequency measured. It can be observed that the standard deviations of the real and imaginary parts of the admittance show a frequency dependence. The latter fact is in agreement with impedance literature on the structure of the standard deviation obtained from the analysis of repeated impedance measurements.[29,39]

The equality of the standard deviations confirms that the variance of the stochastic errors of the real and imaginary parts of the admittance can be assumed to be equal for spectra obtained via DMFA, a property that we exploited in our derivation of Equation (19).

The standard deviations obtained for the redox system range from 0.01 μS at the low frequencies to 10 μS at the high frequencies, while the intercalation system had standard deviations ranging from 8 μS at low frequencies to 40 μS at high frequencies. The correspondence of the mean of $\sigma_Y$ with the experimental data makes it reasonable to assume that our calculated standard deviation captures the frequency dependence of the experimental values. Clearly, changes in the magnitude of the admittance (see supporting information – Figure S12 (a and b)) account to a large extent for the structure of the standard deviation of the admittance. The most visible departure of the experimental results from Equation (19) appears at frequencies less than 100 Hz. The reason for this deviation could not be ascertained. Nevertheless, we could rule out errors arising from spectral leakage and the interference of higher harmonics. Analysis of the experimental data with the a posteriori error determination approach used by Orazem et al.[15,31,44] is presented in Figures S5 and S9 of the supporting information.

The similarity of the stochastic error structure (i.e. how the standard deviation of the real and imaginary parts of the immittance vary as a function of frequency) obtained from the analysis using the transfer function measurement model and the Voigt measurement model are consistent with the findings of Shukla et al.[44] However, our calculated standard deviation differs from the fit of the error structure obtained using the Voigt measurement model at frequencies below 100 Hz (see supporting information, Figures S4, S8, S5 and S9). Furthermore, it has been shown that the error structure is independent of the number of Voigt elements used. Again, this was found for the two systems presented here. When the Padé order was increased to four and five for the redox system and to six and seven for the intercalation system, the standard deviations presented a similar shape when plotted as a function of frequency (see supporting information, Figures S4 and S8).

One limitation of this study relates to the procedure through which the spectra were obtained. This study employs dynamic multi-frequency analysis. If other methods are used for the extraction of the immittance spectra, the underlying formulas have to be taken into account in the derivation of the expression for the variance of the errors. Another caveat implicit in our derivation of the expression for the variance of the error on the admittance is the assumption that the noise in the signal has a constant variance and does not drift. Under this assumption, our theory should perfectly reproduce the error on the immittance.

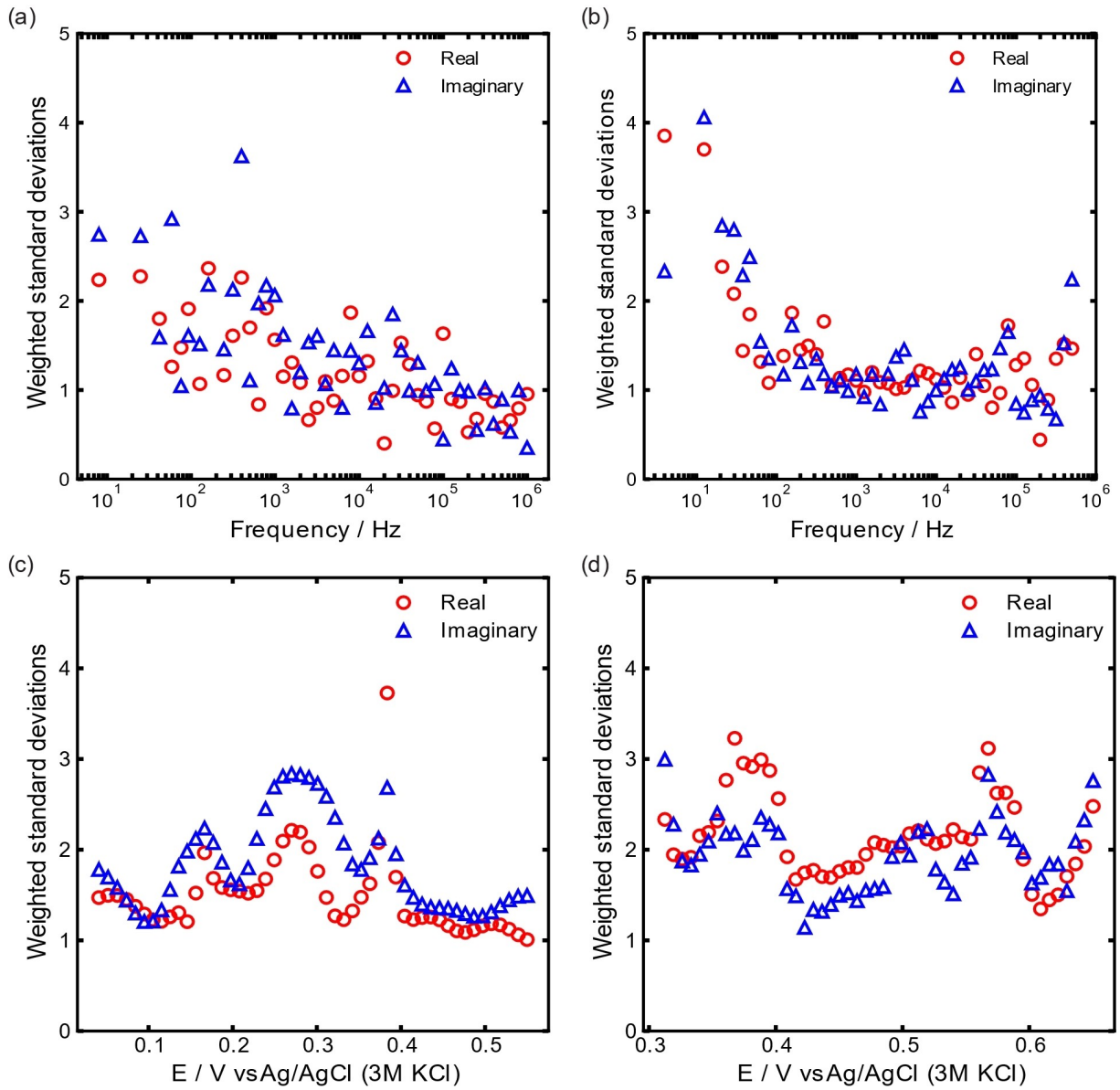


**Figure 5.** (top) weighted standard deviations of the real and imaginary parts of the admittance plotted as a function of frequency for (a) the redox system (b) intercalation system, (bottom) weighted standard deviations of the real and imaginary parts of the admittance plotted as a function of electrode potential for (c) the redox system and (d) for the intercalation system.

## Conclusion

The analysis presented in the study leads to some valuable conclusions, the most important of which is the theoretical development of an expression for the variance of the error on the admittance spectra obtained via DMFA based on the well-established principles of error propagation. According to the calculations, the variance is composed of two components, with one part proportional to the squared absolute value of the admittance. This apriori evaluation eliminates the need for a step by step or trial and error approach towards identifying the stochastic error contribution. The most significant observation of this study is that our calculated standard deviation captures the stochastic noise contribution to admittance spectra obtained via DMFA. Furthermore, the experimentally obtained standard deviations of the real and imaginary components of the error on the admittance are equal – a consequence of the uniform distribution of the errors. Finally, while we believe that the discrepancy that exists between the experimental and calculated standard deviations at frequencies below 100 Hz underestimate the error in the admittance within this region, changing the value of the weights by a factor of two, the effect on the results of the least-squares fit is negligible.

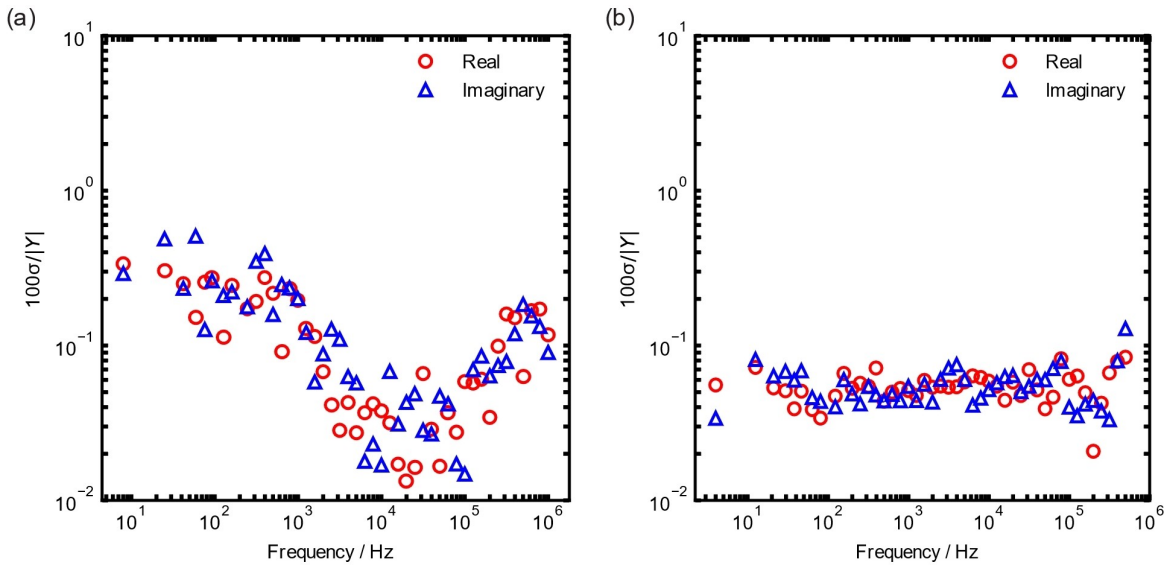


**Figure 6.** Modulus-normalized standard deviations for the real and imaginary parts of the admittance plotted as a function of frequency for (a) the redox and (b) the Intercalation system.

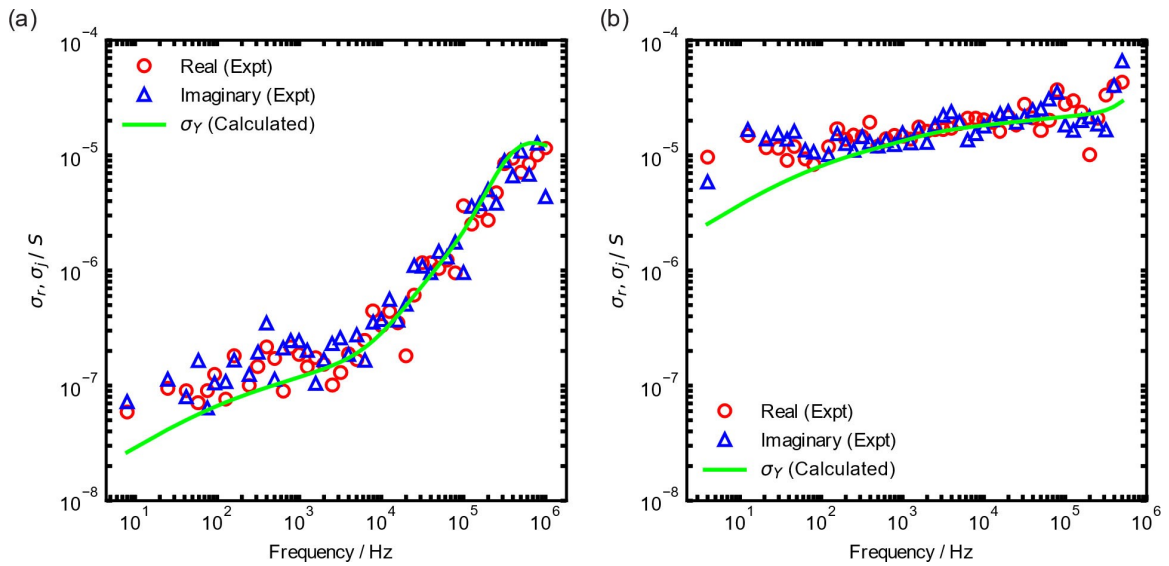


**Figure 7.** Standard deviations for the real and imaginary parts of the admittance plotted as a function for frequency for (a) the redox and (b) the intercalation system. The green line captures the mean of $\sigma_Y$ across the 50 spectra.

## Experimental Section

The intercalation particles used in this study was synthesized using the coprecipitation method.[45] Analytical grade materials were used without further modification. C. Erinmwingbovo[36,46] gives details of the synthesis procedure. Electrochemical measurements were carried out on a Biologic potentiostat. A three-electrode set up with coaxial geometry was employed to mitigate the effects of artefacts arising for cell geometry.[47] The working electrode for the intercalation system consisted of a nickel hexacyanoferrate slurry immobilized on a 3 mm glassy carbon electrode, while a Pt disc working electrode with a diameter of 250 μm was used for the ferric-/ferrocyanide $[Fe(CN)_6]^{3-/4-}$ (5 mM) redox system. The working electrodes were polarized at 275 mV Ag/AgCl/3 M KCl for the ferric-/ferrocyanide $[Fe(CN)_6]^{3-/4-}$ system and 500 mV vs Ag/AgCl/3 M KCl for the intercalation system. The generated quasi-CV wave and the multi-sine from the waveform generator were then used to perturb the electrochemical system. 200 million and 800 million samples were recorded respectively for the redox and intercalation systems while 50 spectra each obtained from the reductive scan were analyzed for both systems. The reference electrode was a low-impedance (20 Ω) Ag/AgCl (3 M KCl) electrode. A bypass configuration consisting of a coil of 0.1 mm platinum wire wound around the tip of the electrode and connected to the reference electrode via a 100 nF capacitor bridge was used to reduce high-frequency artefacts. The dynamic admittance spectra were acquired by perturbation with a multi-sine superimposed on a quasi-CV waveform.[1] The multi-sine waveform was a 5-decade wave with quasi-logarithmically spaced frequencies spanning 1 Mhz to 8 Hz and containing a total of 45 points. A base frequency $F_b$ of 1.0 was used for the redox system, thus a frequency range of 1 MHz to 8 Hz was covered during acquisition while a base frequency $F_b$ of 0.5

was chosen for the intercalation system, equivalent to an acquisition range of 500 KHz to 4 Hz. The intensity of the multi-sine signal was chosen to be 50 mV peak to peak. In order to reduce spectral leakage, the periods of the multi-sine signal and the quasi-CV signal had to be multiples of the sampling time. The other parameters used are shown in Table 1. The voltage perturbation and current response were acquired using a two-channel oscilloscope 4262 Picoscope (Pico technology). The electrolytes consisted of 3 M KCl for redox system and 0.5 M $K_2SO_4$ for the intercalation system. The electrolyte solutions were deaerated before use. For the intercalation system, a slurry consisting of 80:10:10 by weight of nickel hexacyanoferrate particles, carbon C65 (Timcal, Bodio Switzerland), and polyvinylidene fluoride (PVDF) solution in N-methyl-2-pyrrolidone (NMP - Solef S5130, Solvay) was immobilized on a 3 mm glassy carbon electrode using the doctor blade method (200 $\mu m$ ). Prior to coating, the electrode was polished with a 2000 grit emery cloth before use, washed in deionized water, and subject to ultrasound cleaning in a 1:1 solution of water and ethanol. The platinum electrode used for the redox system was prepared in a similar manner with manual polishing using a lapping film of 3 μm, followed by a 2 μm and 1 μm grade (3 M). Final polishing was done using a polishing disc of 0.1 μm grade. Polishing was followed by thorough rinsing with de-ionized water.

## List of abbreviations

| | |
|---|---|
| AIC | Akaike information criterion |
| BIC | Bayesian information criterion |
| CV | cyclic voltammetry |
| dEIS | dynamic electrochemical impedance spectroscopy |
| DMFA | dynamic multi-frequency analysis |
| EIS | electrochemical impedance spectroscopy |

## List of symbols

| | |
|---|---|
| $\delta C_g$ | correlation between the errors on admittances obtained at two frequencies |
| $\delta C_f$ | correlation between the errors on admittances obtained at two different times |
| $\Delta t$ | time interval between two discrete samples |
| $\Delta F$ | frequency interval |
| $\Delta U_{ac}$ | amplitude of the multi-sine signal |
| $\Delta U_{dc}$ | amplitude of the quasi-CV signal |
| $E_h$ | starting potential of the CV |
| $E_b$ | base frequency |
| $F^{-1}$ | inverse discrete-time Fourier transform |
| $f(\Delta i, k_0)$ | Fourier transform of the filter function g |
| $g(k-k_0)$ | band-pass filter function |
| $\tilde{i}_{l,k_0}$ | filtered inverse discrete-time Fourier transform of the acquired current signal around the frequency $k_0$ |
| $I_k$ | discrete-time Fourier transform of the acquired current |
| $i_n$ | discrete samples current response signal |
| $I$ | time index |
| $\hat{L}$ | likelihood estimator |
| $N$ | length of acquired signal |
| $N_s$ | number of admittance scans |
| $n_b$ | a factor which describes the shape of the filter function |
| $n_f$ | number of frequency points |
| $p$ | number of parameters |
| $\sigma^2_{Y_{l,k_0}}$ | expected variance of the error on the admittance |
| $\sigma^2_i$ | variance of the noise on the current response signal |
| $\sigma^2_v$ | variance of the noise on the input voltage signal |
| $\sigma^2_{\mathrm{Re}(Y)}$ | variance of the error on the real part of the admittance |
| $\sigma^2_{\mathrm{Im}(Y)}$ | variance of the error on the imaginary part of the admittance |
| $\sigma_j$ | standard deviation of the imaginary part of the admittance |
| $\sigma_r$ | standard deviation of the real part of the admittance |
| $\theta_{k_0,\Delta n}$ | phase factor |
| Re | real part |
| Im | imaginary part |
| $\tilde{\nu}_{l,k_0}$ | filtered inverse discrete-time Fourier transform of the acquired voltage signal around the frequency $k_0$ |
| $v_n$ | voltage of the working electrode versus the reference electrode |
| $V_k$ | discrete-time Fourier transform of the acquired voltage |
| $w_b$ | bandwidth of the filter function |
| $Y_{l,k_0}$ | dynamic admittance around the frequency $k_0$ |

## Acknowledgements

*The authors gratefully acknowledge the support of the European Research Council (ERC) under the European Union's Horizon 2020 research and innovation program (grant agreement number 772579). Open Access funding enabled and organized by Projekt DEAL. Open Access funding enabled and organized by Projekt DEAL.*

## Conflict of Interest

The authors declare no conflict of interest.

## Data Availability Statement

The data that support the findings of this study are available from the corresponding author upon reasonable request.

**Keywords:** Dynamic impedance spectroscopy · Dynamic multi-frequency analysis (DMFA) · Error propagation · Padé approximants · Statistical analysis

[1] D. Koster, G. Du, A. Battistel, F. La Mantia, *Electrochim. Acta* **2017**, *246*, 553–563.
[2] T. Holm, D. A. Harrington, *ECS Trans.* **2018**, *85*, 167–176.
[3] R. L. Sacci, F. Seland, D. A. Harrington, *Electrochim. Acta* **2014**, *131*, 13–19.
[4] T. Pajkossy, G. Mészáros, *J. Solid State Electrochem.* **2020**, *24*, 2883–2889.
[5] C. Gabrielli, F. Huet, M. Keddam, J. F. Lizee, *J. Electroanal. Chem.* **1982**, *138*, 201–208.
[6] A. Battistel, F. La Mantia, *Electrochim. Acta* **2019**, *304*, 513–520.
[7] A. Battistel, G. Du, F. La Mantia, *Electroanalysis* **2016**, *28*, 2346–2353.
[8] T. Holm, P. K. Dahlstrøm, S. Sunde, F. Seland, D. A. Harrington, *Electrochim. Acta* **2019**, *295*, 139–147.
[9] D. A. Harrington, *ECS Trans.* **2013**, *45*, 3–14.

[10] C. Erinmwingbovo, D. Koster, D. Brogioli, F. La Mantia, *ChemElectroChem* **2019**, vol 6, issue 21, 5387–5395.
[11] C. Erinmwingbovo, F. La Mantia, *Sci. Rep.* **2021**, *11*, 1362.
[12] F. Ciucci, *Curr. Opin. Electrochem.* **2019**, *13*, 132–139.
[13] D. A. Harrington, P. Van Den Driessche, *Electrochim. Acta* **2011**, *56*, 8005–8013.
[14] P. Agarwal, M. E. Orazem, L. H. Garcia-Rubio, *J. Electrochem. Soc.* **1992**, *139*, 1917–1927.
[15] P. Agarwal, O. D. Crisalle, M. E. Orazem, L. H. Garcia-Rubio, *J. Electrochem. Soc.* **1995**, *142*, 4149–4158.
[16] P. Agarwal, M. E. Orazem, L. H. Garcia-Rubio, *J. Electrochem. Soc.* **1995**, *142*, 4159–4168.
[17] L. Pauwels, W. Simons, A. Hubin, J. Schoukens, R. Pintelon, *Electrochim. Acta* **2002**, *47*, 2135–2141.
[18] G. A. Baker, P. Graves-Morris, *Padé Approximants Second Edition*, Cambridge University Press, Cambridge, **1996**.
[19] P. Zoltowski, *Solid State Ionics* **2005**, *176*, 1979–1986.
[20] E. Van Gheem, E. Tourwé, R. Pintelon, A. Hubin, *J. Electroanal. Chem.* **2008**, *613*, 186–192.jansen.
[21] P. Zoltowski, *J. Electroanal. Chem.* **1994**, *375*, 45–57.
[22] A. Sadkowski, *J. Electroanal. Chem.* **2004**, *573*, 241–253.
[23] W. Watson, M. E. Orazem, *EIS Meas. Model Program*, DOI 10.1149/osf.io/kze9x can be found under ecsarxiv.org/kze9x, **2020**.
[24] J. R. Macdonald, *Electrochim. Acta* **1990**, *35*, 1483–1492.
[25] J. R. Dygas, M. W. Breiter, *Electrochim. Acta* **1999**, *44*, 4163–4174.
[26] M. Ingdal, R. Johnsen, D. A. Harrington, *Electrochim. Acta* **2019**, *317*, 648–653.
[27] M. E. Orazem, P. Agarwal, A. N. Jansen, P. T. Wojcik, L. H. Garcia-Rubio, *Electrochim. Acta* **1993**, *38*, 1903–1911.
[28] P. Zoltowski, *J. Electroanal. Chem. Interfacial Electrochem.* **1984**, *178*, 11–19.
[29] J. R. Jennings, Q. Wang, *J. Electrochem. Soc.* **2012**, *159*, F141–F149.
[30] A. N. Jansen, P. T. Wojcik, P. Agarwal, M. E. Orazem, *J. Electrochem. Soc.* **1996**, *143*, 4066–4074.
[31] M. E. Orazem, P. Agarwal, C. Deslouis, B. Tribollet, *J. Electrochem. Soc.* **1996**, *143*, 948–960.
[32] M. E. Orazem, P. Agarwal, L. H. Garcia-Rubio, *J. Electroanal. Chem.* **1994**, *378*, 51–62.
[33] M. E. Orazem, *J. Electroanal. Chem.* **2004**, *572*, 317–327.
[34] T. Yokoshima, D. Mukoyama, K. Nakazawa, Y. Gima, H. Isawa, H. Nara, T. Momma, T. Osaka, *Electrochim. Acta* **2015**, *180*, 922–928.
[35] Y. Koç, U. Morali, S. Erol, H. Avci, *Turk. J. Chem.* **2021**, *45*, 1895–1915.
[36] C. Erinmwingbovo, D. Koster, D. Brogioli, F. La Mantia, *ChemElectroChem* **2019**, *6*, 5353.
[37] J. Libii, in *Gibbs Phenom. Its Appl. Sci. Eng.*, Portland, Oregon, **2005**.
[38] J. R. Taylor, in *An Introd. to Error Anal. Study Uncertainties Phys. Meas.*, University Science Books, Sausalto, California, **1996**, pp. 146–148.
[39] S. L. Carson, M. E. Orazem, O. D. Crisalle, L. García-Rubio, *J. Electrochem. Soc.* **2003**, *150*, E477.
[40] H. Akaike, *IEEE Trans. Autom. Control* **1974**, *19*, 716–723.
[41] H. Akaike, *Ann. Inst. Stat. Math.* **1978**, *30*, 9–14.
[42] K. Darowicki, A. Zieliński, J. Ryl, P. Slepski, *Electrochim. Acta* **2013**, *87*, 930–939.
[43] K. Burnham, D. R. Anderson, *J. Wildl. Manage.* **2003**, *67*, 655.
[44] P. K. Shukla, M. E. Orazem, O. D. Crisalle, *Electrochim. Acta* **2004**, *49*, 2881–2889.
[45] C. D. Wessells, S. V. Peddada, R. A. Huggins, Y. Cui, *Nano Lett.* **2011**, *11*, 5421–5425.
[46] C. Erinmwingbovo, M. S. Palagonia, D. Brogioli, F. La Mantia, *ChemPhysChem* **2017**, *18*, 917–925.
[47] A. Battistel, M. Fan, J. Stojadinović, F. La Mantia, *Electrochim. Acta* **2014**, *135*, 133–138.

Manuscript received: January 28, 2022
Revised manuscript received: April 8, 2022
Accepted manuscript online: April 11, 2022